Proton Transfer Mechanisms in Bimetallic Hydrogenases

Hulin Tai,[†] Shun Hirota,[,‡] and Sven T. Stripp[*,§]*

[†] MOE Key Laboratory of Natural Resources of the Changbai Mountain and Functional Molecules, Department of Chemistry, Yanbian University, Yanji 133002, Jilin, China

[‡] Division of Materials Science, Graduate School of Science and Technology, Nara Institute of Science and Technology, Ikoma, Nara 630-0192, Japan

[§] Bioinorganic Spectroscopy, Department of Physics, Freie Universität Berlin, 14195 Berlin, Germany

Corresponding Authors

*E-mail: hirota@ms.naist.jp

*E-mail: sven.stripp@fu-berlin.de

Contents

Conspectus

Hydrogenases are iron-sulfur enzymes that catalyze proton reduction and H_2 oxidation with outstanding efficiency. They are considered blueprints for the design of transition metal complexes, *e.g.* as heterogenous catalysts in the context of H_2 production from water. Moreover, hydrogenases are biological model systems for metal hydride chemistry and proton-coupled electron transfer.

Depending on the composition of the active site cofactor, [NiFe]-hydrogenases are distinguished from [FeFe]-hydrogenases. The former binds a hetero bimetallic nickel/iron site, embedded in the protein by four cysteine ligands. The later, by contrast, carries a homo bimetallic iron/iron site attached to the protein by only a single cysteine. Carbon monoxide and cyanide ligands (CO/CN) at the active site facilitated detailed investigations of hydrogenase catalysis by infrared spectroscopy, owing to strong signals and redox-dependent frequency shifts. However, the details of proton transfer have not been addressed experimentally.

We found that specific redox state transitions in [NiFe]- and [FeFe]-hydrogenase can be triggered by visible light to record extremely sensitive 'light-minus-dark' infrared difference spectra monitoring key amino acid residues as shown in the ToC figure. As these transitions are coupled to protonation changes, our data allowed investigating dynamic hydrogen-bonding changes that go well beyond the resolution of protein crystallography.

In [NiFe]-hydrogenase, photolysis of the bridging hydride ligand in the 'Ni-C' state was followed by rapid accumulation of the 'Ni-SI$_a$' state and/or 'Ni-L' state. Infrared difference spectra in various isotopic media clearly indicated the formation of a protonated cysteine residue as well as hydrogen-bonding changes involving the COOH group of a glutamic acid residue and a 'dangling water' molecule. These findings are in excellent agreement with crystallographic analyses of [NiFe]-hydrogenase in the Ni-R state and allowed devising a molecular precise model of catalytic proton transfer.

In [FeFe]-hydrogenase, an external redox dye was used to accumulate the 'Hred' state over the oxidized resting state 'Hox'. Infrared difference spectra of wild-type enzyme and numerous amino acid variants indicated hydrogen-bonding changes involving the COOH groups of two glutamic

acid residues. Moreover, we noted the deprotonation of an arginine residue. Crystallographic analyses of [FeFe]-hydrogenase in the Hox state failed to explain the rapid proton transfer due to a 'breach' in the succession of residues. To this end, our findings facilitated a molecular precise model of 'discontinued' proton transfer.

The comparison of catalytic proton transfer in bimetallic hydrogenases emphasizes the role of the outer coordination sphere. We suggest that the stable protonation of a nickel-ligating cysteine in [NiFe]-hydrogenase has a crucial influence on the preferred direction of proton flow and catalysis (i.e., H$_2$ oxidation). On the contrary, proton transfer in [FeFe]-hydrogenase involves an adjacent cysteine as a relay group that promotes both proton release and proton uptake. We presume that this causes the notable bidirectionality of [FeFe]-hydrogenase. These observations must guide the design of biomimetic compounds for the production or consumption of H$_2$.

Table of Contents
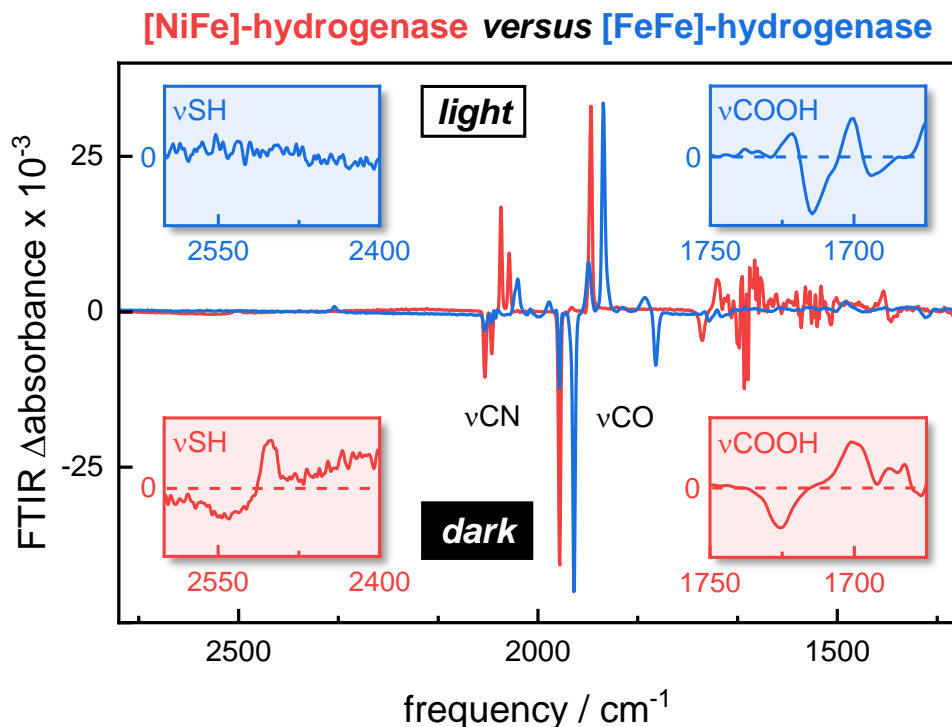
1. Introduction

Hydrogenases are iron-sulfur enzymes that catalyze hydrogen turnover in archaea, bacteria, and algae. Three phylogenetically independent classes have been described: [NiFe]-hydrogenase, [FeFe]-hydrogenase, and [Fe]-hydrogenase.[1] In general, the bimetallic [NiFe]- and [FeFe]-hydrogenases show higher catalytic activities than [Fe]-hydrogenase and catalyze both H_2 oxidation and proton reduction.[1–3] The reaction includes a hydride intermediate (heterolytic hydrogen turnover, **Eq. 1**):

Eq. 1 $\qquad\qquad\qquad\qquad H_2 \rightleftharpoons [H^+ + H^-] \rightleftharpoons 2H^+ + 2e^-$

The active site cofactors of bimetallic hydrogenases inspired numerous biomimetic compounds designed to cleave H_2 (*e.g.*, in electrochemical half cells) or produce H_2 as a 'green fuel'.[4–6] But while the Ni−Fe and Fe−Fe cofactors have been characterized by X-ray diffractometry (XRD), electron paramagnetic resonance (EPR) spectroscopy, Fourier-transform infrared (FTIR) spectroscopy, and other techniques[1], the details of proton transfer were unraveled only recently.[7,8] The novel findings, collected independently in our laboratories, emphasize the importance of the 'outer' coordination sphere and the selective supply and detraction of protons.

Standard [NiFe]-hydrogenases are comprised of two subunits.[9,10] The small subunit binds three iron-sulfur clusters, termed proximal, medial, and distal relative to the position of the Ni−Fe site (**Figure 1A**). These clusters facilitate electron transfer between the protein surface and the active site cofactor. The Ni−Fe site is anchored to the large subunit by four cysteine residues: two terminal ligands to the nickel ion and two bridging ligands between the nickel and iron ions (**Figure 1B**).[9] The iron ion is further coordinated by one carbon monoxide (CO) and two cyanide (CN^-) ligands and an additional ligand that may bind in the Ni−Fe bridging position.[1,2] The Ni−Fe

site exists in several redox states (**Figure 1C**): the nickel ion changes its oxidation state (*i.e.*, Ni^{3+}, Ni^{2+}, and Ni^{+}) during the catalytic cycle whereas the low-spin iron ion retains the ferrous state ($S = 0$, Fe^{2+}).[2,4] There are several well-conserved amino acid residues close to the Ni−Fe site (**Figure 1B**), which have been proposed to play important roles in the catalytic reaction of [NiFe]-hydrogenase (**Eq. 1**).[2,4,9,11]
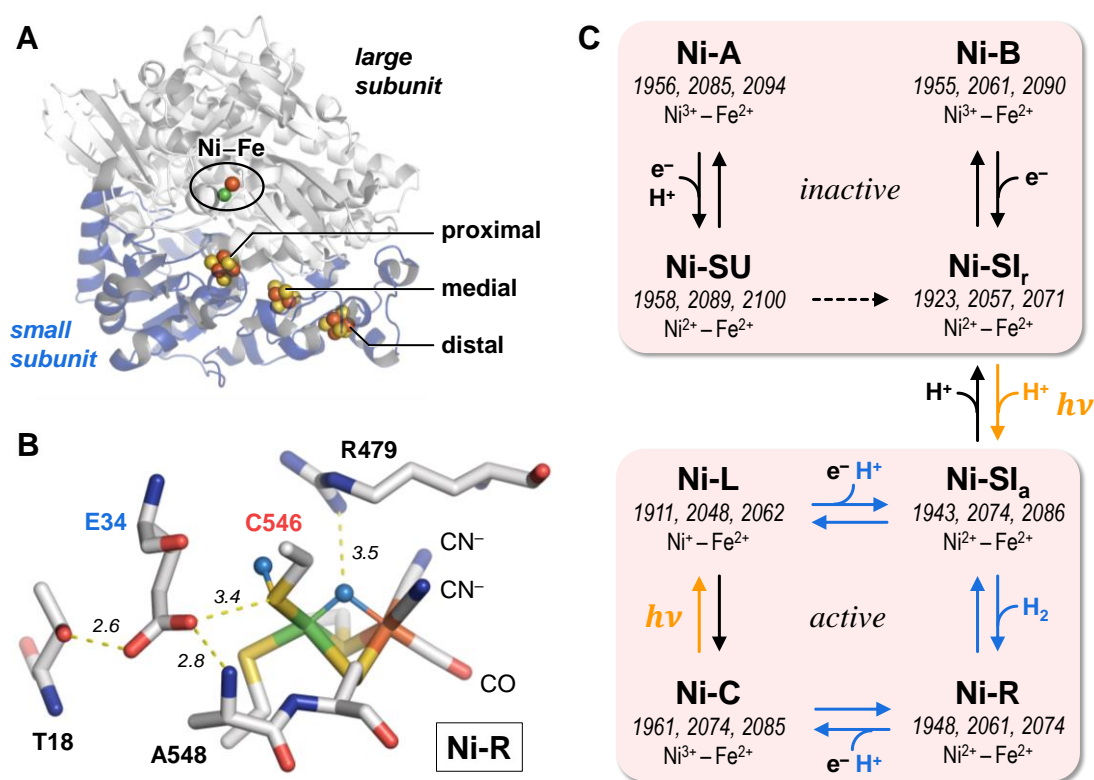
Figure 1 – [NiFe] hydrogenase. (A) X-ray crystal structure of the [NiFe]-hydrogenase from *Dv*MF (pdb coordinates 4U9H). The Ni–Fe site and the proximal, medial, and distal iron-sulfur clusters are highlighted. **(B)** Ni–Fe site in the **Ni-R** state and proton transfer pathway (distances in Å). The μH^- ligand and the extra proton at C546 are shown as light blue spheres. **(C)** Reaction scheme of [NiFe]-hydrogenase including the formal charges of the Ni–Fe site. The CO and CN^- stretching frequencies of the [NiFe]-hydrogenase from *Dv*MF are given in cm^{-1}. Note that the **Ni-SI$_r$** and **Ni-C** states are sensitive to visible light (orange arrows). Blue arrows depict catalytic proton transfer. The dashed arrow marks a speculative transition.

Standard [FeFe]-hydrogenases are comprised of two domains.[12,13] The 'F-domain' binds up to five iron-sulfur clusters that facilitate electron transfer between the protein surface and the active site cofactor (**Figure 2A**). In the 'H-domain', four cysteines residues anchor the active site cofactor or 'H-cluster': three terminal ligands to a [4Fe-4S] cluster and a single bridging ligand between the [4Fe-4S] cluster and the Fe−Fe site (**Figure 2B**). The latter is coordinated by up to four CO ligands, two CN^- ligands, and an aminodithiolate ligand (adt) that bridges Fe_p and Fe_d ('p' refers to proximal and 'd' refers to distal iron ion, relative to the [4Fe-4S] cluster).[12–14] The H-cluster exists in several redox states (**Figure 2C**): the Fe−Fe site changes between 'super-oxidized' ($Fe_p^{2+}-Fe_d^{2+}$), oxidized mixed-valence ($Fe_p^{2+}-Fe_d^{+}$), and formally reduced states ($Fe_p^{+}-Fe_d^{+}$), whereas the low-potential [4Fe-4S] cluster changes between oxidized (+2) and reduced (+1) states.[3] There are several well-conserved amino acid residues and water molecules that connect the Fe−Fe site to the protein surface (**Figure 2B**), which have been shown to play important roles in the catalytic reaction of [FeFe]-hydrogenase (**Eq. 1**).[15–17]
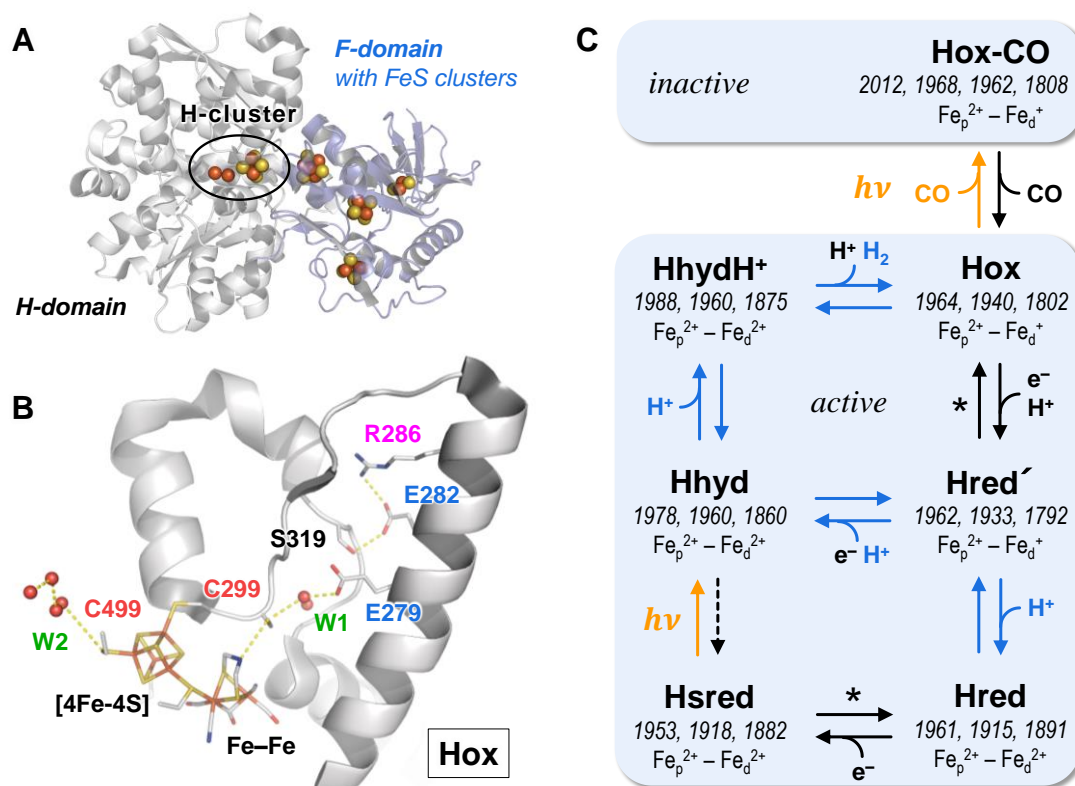
Figure 2 – [FeFe]-hydrogenase. (**A**) X-ray crystal structure of the [FeFe]-hydrogenase from *Cp*I (pdb coordinates 4XDC). The H-cluster and accessory iron-sulfur clusters are highlighted. (**B**) The H-cluster in the **Hox** state and proton transfer pathway. The Fe–Fe site is connected to the protein surface by a conserved trajectory of amino acid residues and water molecules (W1). Additionally, a chain of water molecules (W2) connects the protein surface and the [4Fe-4S] cluster. (**C**) Reaction scheme including the formal charges of the Fe–Fe site. The CO and CN^- stretching frequencies of *Cr*HydA1 are given in cm^{-1}. The asterisk highlights redox/protonation changes at the [4Fe-4S] cluster. Note that the **Hox** and **Hsred** states are sensitive to visible light (orange arrows). Blue arrows depict catalytic proton transfer. The dashed arrow marks a speculative transition.

In this account, we will review recent progress in the understanding of catalytic and regulatory proton transfer in bimetallic hydrogenases. We will discuss how proton transfer (PT) and proton-coupled electron transfer (PCET) influence the formation of key redox states in [NiFe]-hydrogenase (Chapter 2) and [FeFe]-hydrogenase (Chapter 3). The high-resolution crystal structures available for bimetallic hydrogenases represent the basis on which potential PT trajectories have been discussed and simulated.[18–21] Going beyond the scope of XRD, we will focus on FTIR difference spectroscopy unraveling the subtle changes when switching between different states. Infrared spectroscopy allows interrogating chemical entities involved in PT directly, *e.g.*, cysteine, glutamic/aspartic acid, and arginine residues as well as individual H_2O molecules ('dangling water').[22] Although hydrogenases do not carry a catalytic chromophore, visible light can be used to trigger protonation changes, *e.g.*, by photolyzing bridging hydride ligands or exciting redox dyes that initiate PCET.[7,8] The account will close on a discussion of similarities and differences between bimetallic hydrogenases (Chapter 4).

2. Proton transfer in [NiFe]-hydrogenase

2.1 Light sensitivity of the Ni–Fe active site

The **Ni-SI$_r$** and **Ni-C** states of the [NiFe]-hydrogenase from *Desulfovibrio vulgaris* Miyazaki F (*Dv*MF) converted to **Ni-SI$_a$** upon laser irradiation at 514.5 nm under cryogenic conditions.[23,24] **Ni-C** converted to **Ni-SI$_a$** *via* **Ni-L** when the proximal [4Fe-4S] cluster was oxidized (2+) but only to **Ni-L** when it was reduced (1+).[24] These photoconversions allowed obtaining 'light-minus-dark' FTIR difference spectra and facilitated investigating the PT mechanism of [NiFe]-hydrogenase.

In the absence of O_2, **Ni-SI$_a$** converts to the inactive **Ni-B** state upon one-electron oxidation and insertion of a bridging hydroxo (μOH^-) ligand at the Ni−Fe site ('anaerobic inactivation').[2,9] This process includes **Ni-SI$_r$** as a transient intermediate. The acid−base equilibrium between **Ni-SI$_a$** and **Ni-SI$_r$** is a common feature among [NiFe]-hydrogenases and the equilibrium exhibits a pK_a value of about 8.[1,2] Two models have been proposed to explain this behavior (**Figure 3**): In the first model, the μOH^- ligand exists in **Ni-SI$_r$** and leaves the Ni−Fe site upon protonation as a water molecule, producing **Ni-SI$_a$**. In the second model, **Ni-SI$_r$** accepts a proton at the terminal Ni^{2+}-coordinating cysteine side chain (C546 in *Dv*MF, compare **Figure 1B**). Recently, we have shown that C546 is deprotonated in the conversion of **Ni-L** to **Ni-SI$_a$** (Chapter 2.2), which excludes the second mechanism.[7]
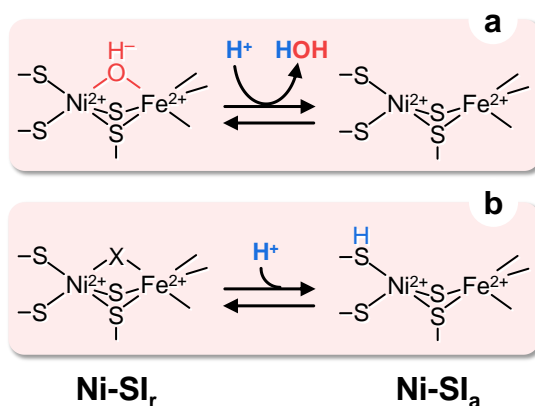
Figure 3 – Anaerobic inactivation of [NiFe]-hydrogenase. The two proposed models for the equilibrium between **Ni-SI$_r$** and **Ni-SI$_a$**. (a) The first model is characterized by the dissociation/association of the μOH^- ligand. (b) The second model comprises the protonation of a coordinating cysteine. 'X' may be OH^-, H_2O, or empty.

The PT dynamics for the equilibrium between **Ni-SI$_r$** and **Ni-SI$_a$** have been identified utilizing dark adaption after irradiation of **Ni-SI$_r$** under cryogenic conditions.[25] The back reaction of **Ni-SI$_a$** into **Ni-SI$_r$** in H_2O and D_2O was described by first-order kinetics. Moreover, a huge activation energy value ($E_a \approx 65$ kJ mol^{-1}) and a large kinetic isotope effect ($k_H/k_D = \sim150$) were determined, which simple S−H bond cleavage cannot explain.[26] Rather, the results indicate that the conversion of **Ni-Sl$_a$** to **Ni-SI$_r$** is an intricate reaction supporting the first model, in which the conversion requires not only the transfer of a water molecule into the Ni−Fe site but also the extraction of a proton from a water molecule (**Figure 3**).

2.2 Proton transfer during the catalytic cycle

The Ni−Fe site adopts several oxidation states during the catalytic cycle, namely **Ni-SI$_a$** (Ni^{2+}), **Ni-R** (Ni^{2+}), **Ni-C** (Ni^{3+}), and **Ni-L** (Ni^{+}).[2] These states convert among each other by addition or release of H_2, protons, and/or electrons (**Figure 1C**). The catalytic reaction mechanism at the Ni−Fe site of [NiFe]-hydrogenase is rather well understood; however, the mechanism of catalytic PT is still under debate.[2,4,9,11]

The primary proton acceptor during the catalytic oxidation of H_2 has been proposed by structural[9] and theoretical studies.[19,27] Following this model, one proton is transferred from the Ni−Fe site to a terminal Ni-coordinating cysteine (*i.e.*, C546 in *Dv*MF), which may act as the entry point of the PT pathway.[9,19] Mutagenesis studies have shown that a conserved glutamic acid residue (*i.e.*, E34 in *Dv*MF) located close to C546 is also important for the PT during the catalytic reaction.[28–31] For example, variation of E25 to glutamine in the [NiFe]-hydrogenase from *Desulfovibrio fructosovorans* (eq. E34 in *Dv*MF) resulted in a decrease of H_2 oxidation activity to less than 0.1%.[28] Greene *et al.* showed by time-resolved IR spectroscopic studies that E17 in the O_2-tolerant

[NiFe]-hydrogenase from *Pyrococcus furiosus* (eq. E34 in *Dv*MF) is a proton donor/acceptor for the interconversion between **Ni-C** and **Ni-SI$_a$**.[29]

We have reported the first spectroscopic evidence for the changes in the protonation state of the C546 ligand and the E34 side chain near the Ni−Fe site of *Dv*MF [NiFe]-hydrogenase.[7] We recorded cryogenic FTIR difference spectra by utilizing the light-induced conversion of **Ni-C** (negative bands) into **Ni-L** (positive bands). Positive SH and SD stretching bands were observed at 2505 and 1822 cm^{-1} (**Figure 4**, spectra a/b), respectively, and could be assigned to C546 of **Ni-L**.[7] Similar frequencies for metal-coordinated thiols have been observed in Ni−Fe and Fe−Fe model compounds.[32,33] Moreover, computational studies have shown that C546 is most easily protonated among all the cysteine ligands, resulting in stabilization of −32.5 kJ mol^{-1} in **Ni-L**.[27] Interestingly, no SH stretching band was observed for **Ni-C** and **Ni-SI$_a$**, indicating that the C546 is deprotonated in these states.[7] Temperature-dependent FTIR studies on the equilibrium between C546-SH and C546-S$^-$ in **Ni-L** suggest ΔH and ΔS values of 6.4 ± 0.8 kJ mol^{-1} and 25.5 ± 10.3 J mol^{-1} K^{-1}, which indicates efficient PT at the Ni−Fe site.[34] In sum, these results strongly support the hypothesis that the sulphur atom of C546 is a proton acceptor/donor for the conversion of **Ni-C** to **Ni-SI$_a$** *via* **Ni-L** in *Dv*MF [NiFe]-hydrogenase.
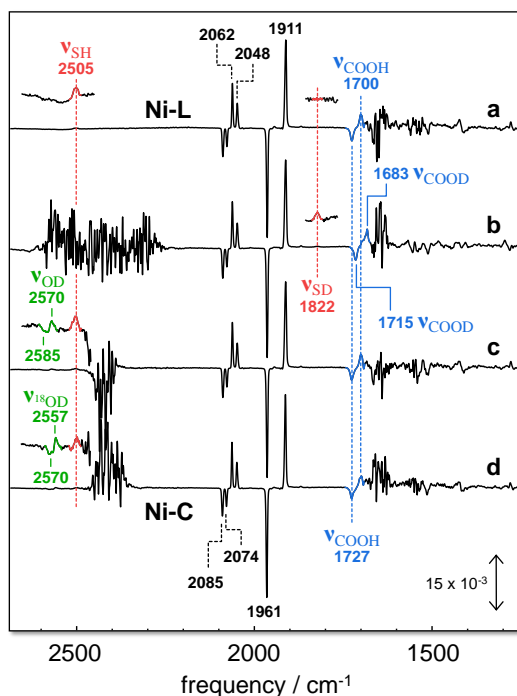
Figure 4 – FTIR difference spectra of the Ni-C → Ni-L transition. The data shows the difference between the spectra after and before light irradiation at 138 K and pH/D 7.0. Conditions: **(a)** H_2/H_2O. **(b)** D_2/D_2O. **(c)** D_2/H_2O. **(d)** $D_2/H_2^{18}O$. Magnified spectra (×10) in the 1765−1855 and 2460−2655 cm^{-1} regions are also shown. The intensities of the spectra were normalized according to the intensities of the ν_{CO} bands in spectrum (a). Legend: $\nu_{CO/CN}$ (black), $\nu_{COOH/D}$ (blue), $\nu_{SH/D}$ (red), ν_{OD} and ν_{18OD} (green). Copyright 2019 Wiley-VCH.

Positive and negative C=O stretching frequencies of **Ni-L** and **Ni-C** were observed at 1700 and 1727 cm^{-1}, respectively, and found to be shifted to lower frequencies of 1683 and 1715 cm^{-1} in the deuterated sample (**Figure 4**, spectra a/b).[7] These bands were assigned to E34 (**Figure 1B**). The C=O stretching frequencies of carboxylic groups (ν_{COOH}) under different environments have been estimated by combined theoretical and experimental studies.[22] Here, lower frequencies suggest stronger hydrogen bonding, *i.e.* shorter distances and/or multiple partners. For **Ni-C** and **Ni-L**, ν_{COOH} were observed at 1727 and 1700 cm^{-1}, respectively, indicating that the E34 forms two

13

hydrogen bonds in **Ni-L** (through the OH hydrogen and the C=O oxygen of the COOH side chain) and a single hydrogen bond in **Ni-C** (through the OH hydrogen). As **Ni-SI$_a$** shows v_{COOH} similar to **Ni-C**, E34 apparently exhibits a single hydrogen bond in **Ni-SI$_a$** as well.[7]

In the **Ni-C → Ni-L** difference spectrum of D_2/H_2O-prepared *Dv*MF [NiFe]-hydrogenase, an additional feature at 2570 cm^{-1} and 2585 cm^{-1} was observed (**Figure 4**, spectrum c).[7] These bands shifted to lower frequencies of 2557 and 2570 cm^{-1}, respectively, for the enzyme prepared in D_2/$H_2^{18}O$ (**Figure 4**, spectrum d). The observed isotope shifts (~14 cm^{-1}) were in good agreement with the increase in mass from ^{16}O to ^{18}O and facilitates assignment to a 'dangling water'.[22] Such a water molecule may exists near the Ni−Fe site, changing its orientation by realignment of the hydrogen-bonding network around C546 and E34 upon conversion of **Ni-C** to **Ni-L**.

2.3 Understanding [NiFe]-hydrogenase catalysis

Our spectroscopic results and the high-resolution crystal **Ni-R** structure of *Dv*MF [NiFe]-hydrogenase strongly indicate that the terminal, nickel-coordinated cysteine C546 is the primary proton donor/acceptor.[7,9] Further, we found that the gradual realignment of the hydrogen-bonded network between C546, E34, A548, and T18 is essential for the efficient PT among **Ni-C**, **Ni-L**, and **Ni-SI$_a$** in the catalytic cycle of [NiFe]-hydrogenase (**Figure 1C**).[7,9] We propose that the catalytic reaction proceeds as follows:

In the first step, H_2 is cleaved heterolytically (**Eq. 1**). This leads to the transition of the oxidized **Ni-SI$_a$** to the fully-reduced **Ni-R** that is characterized by a μH^- ligand at the Ni–Fe site and a protonated C546-SH as the primary proton acceptor for the heterolytic cleavage of H_2 (**Figure 5**).[9] According to crystallographic analyses, E34-COOH and threonine T18 form a low-barrier hydrogen bond in **Ni-R** of *Dv*MF [NiFe]-hydrogenase (**Figure 5**).[9] The bond lengths between the

14

C atom and two O atoms of the E34 side chain are 1.29 and 1.22 Å and one of the E34 O atoms sits 2.58 Å away from the O atom of the T18 side chain in **Ni-R** (**Figure 1B**), suggesting the involvement of these residues in the PT pathway. It is reasonable to assume that E34-COOH is additionally hydrogen-bonded to A548-NH in **Ni-R**.[9] *In the second step,* **Ni-C** is produced by one-electron oxidation of **Ni-R** (**Figure 5**).[7] **Ni-C** is also characterized by a μH^- ligand[35] but deprotonated at C546 and forms a single hydrogen bond to E34-COOH.[7] The proton formerly bound to C546 may transfer to the nearby E34 during the conversion of **Ni-R** to **Ni-C** and the E34-COOH is hydrogen-bonded to C546 in **Ni-C**. *In the third step,* C546-SH is restored by oxidation of the μH^- at the Ni−Fe site of **Ni-C**, resulting in formation of **Ni-L** (**Figure 5**).[35] Reprotonation of C546 in **Ni-L** has been demonstrated by the direct observation of the SH stretching frequency at 2505 cm^{-1} (**Figure 4**, spectrum a).[7] The detected down-shift of the carboxylic C=O stretching frequency is well compatible with E34 forming hydrogen bonds to both T18-OH and A548-NH. *In the fourth step,* one-electron oxidation of **Ni-L** restores **Ni-SI$_a$**, accompanied with the release of a proton from C546-SH, and the formation of a hydrogen bond between E34-COOH and C546-S$^-$. Note the similar PT mechanism between the *first* and *third steps* as well as between the *second* and *fourth steps*.
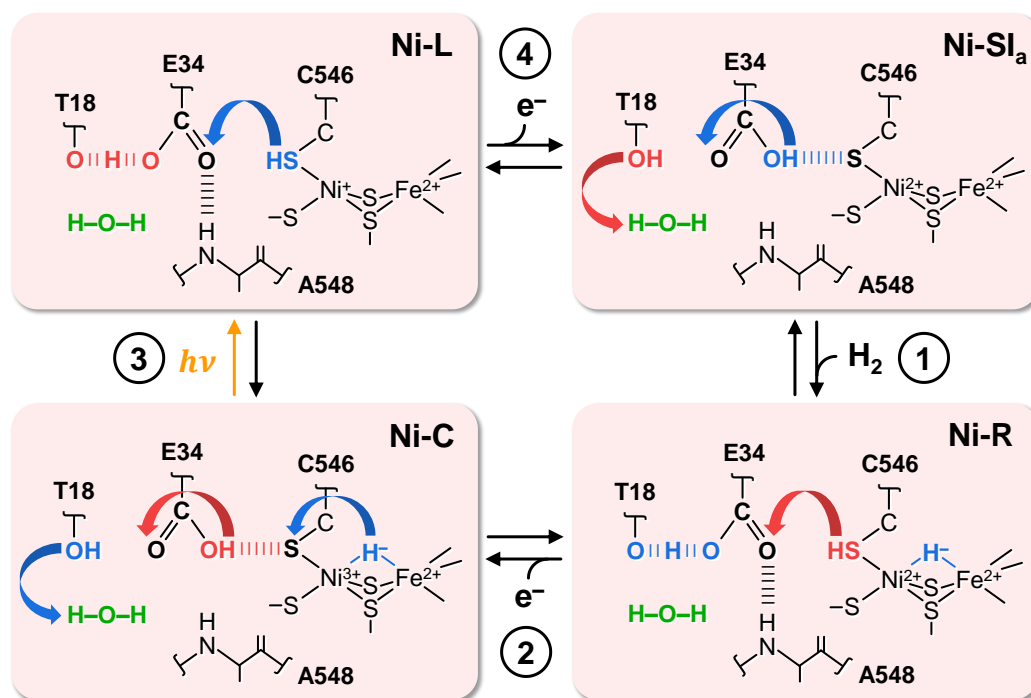
Figure 5 – Proposed proton transfer mechanism of [NiFe]-hydrogenase. (1) Upon binding to **Ni-SI$_a$**, H$_2$ is cleaved heterolytically and **Ni-R** is formed. A low-barrier hydrogen bond is found between E34 and T18 (vertical dashes). (2) The oxidative formation of **Ni-C** is accompanied by PT to T18 and E34. Moreover, FTIR spectroscopy identified hydrogen-bonding changes involving a 'dangling water'. (3) Upon conversion into **Ni-L**, the μH$^-$ ligand is lost to re-protonate C546. (4) The oxidative formation of **Ni-SI$_a$** is accompanied by PT to T18 and E34.

Several well-conserved water molecules are located near E34 and T18 in the crystal structure of *Dv*MF [NiFe]-hydrogenase.[9] As discussed above, the FTIR data in **Figure 4** (spectrum c) strongly suggest that a 'dangling water' near the Ni–Fe site may play an integral part in the PT pathway.[7] A proton may transfer easily from an amino acid (*e.g.*, T18) to the 'dangling water' during the catalytic reaction (**Figure 5**). There are well conserved amino-acid residues (E16, H36, D28, and R38 in *Dv*MF sequence) and several water molecules in similar positions in [NiFe]-hydrogenase, indicating their possible involvement in the PT pathway.[9] Additionally, the conversion of **Ni-L**

16

into **Ni-SI$_a$** (*step four*) was observed only when the proximal [4Fe-4S] cluster was oxidized; thus, the [4Fe-4S] cluster may function as a gatekeeper for PCET between the Ni–Fe site and external redox partner.[24]

2.4 Alternative proton transfer pathways

An alternative PT pathway *via* the conserved arginine R509 (R479 in *Dv*MF, compare **Figure 1B**) has been proposed in the O$_2$-tolerant [NiFe]-hydrogenase from *Escherichia coli* (*Ec*).[36] This residue was suggested to function together with the active site as a frustrated Lewis pair to polarize and heterolytically cleave H$_2$. The positively charged guanidium group of the arginine side chain may act as counterion to μH$^-$ in **Ni-R** and **Ni-C**, and this interaction is essential for the catalytic activity of [NiFe]-hydrogenase.[29] On the contrary, Yu *et al.* reported a terminal thiol-dominated H/D exchange between H$_2$ and deuterated solvents in a diiron model complex.[33] The strong acidic character of the terminal thiol facilitated fast proton exchange, clearly supporting the 'thiol-hydride'-based mechanism for heterolytic cleavage of H$_2$ in [NiFe]-hydrogenase.[9,29]

Evans *et al*. reported that the catalytic cycle of the E28Q variant of the O$_2$-tolerant *Ec* [NiFe]-hydrogenase was dominated by the reduced **Ni-R** and **Ni-C**, concluding that E28 (equivalent E34) is essential for the process occurring *after* formation of **Ni-C**.[30] However, an additional PT pathway may be necessary for the transition of **Ni-R** to **Ni-C** in the E28Q variant. For example, an alternative 'histidine' pathway, connecting the Ni−Fe site and the proximal [4Fe-3S] cluster, has been proposed in the O$_2$-tolerant [NiFe]-hydrogenase from *Cupriavidus necator* (formerly *Ralstonia eutropha*).[37,38] Further studies are necessary to elucidate the comprehensive PT mechanism for the conversion of **Ni-R** to **Ni-C**.

3. Proton transfer in [FeFe]-hydrogenase

3.1 Light sensitivity of the Fe−Fe active site

Both parts of the H-cluster, the Fe−Fe site and the [4Fe-4S] cluster, react to UV/vis irradiation. For example, several studies have shown that the active-ready, oxidized **Hox** state converts into the CO-inhibited, oxidized **Hox-CO** state upon illumination.[39–41] This reaction is caused by the sensitivity of metal carbonyl complexes to visible light.[42–44] The conversion of **Hox** into **Hox-CO** is independent of pH and no significant changes in the carboxylic regime were detected by FTIR difference spectroscopy.[8]

Illuminating oxidized [FeFe]-hydrogenase with high intensity visible light under cryogenic conditions, resonance Raman spectroscopy revealed a one-electron reduction of the [4Fe-4S] cluster (**Hox → Hred´**).[45] Under ambient conditions, this redox conversion shows a clear dependence on pH and has been explained by a concerted protonation of a cysteine residue that coordinates to the [4Fe-4S] cluster (most likely C499, compare **Figure 2B**).[46,47] Notably, no significant changes in the carboxylic regime were detected by FTIR difference spectroscopy for the conversion of **Hox** into **Hred´**.[8] This is in agreement with PCET as protons are likely to proceed *via* a chain of 'conserved' water molecules (W2 in **Figure 2B**) that connect the [4Fe-4S] cluster to the protein surface.[47] The W2 trajectory may have regulatory functions and must not be described as an 'alternative' PT pathway (Chapter 3.4).
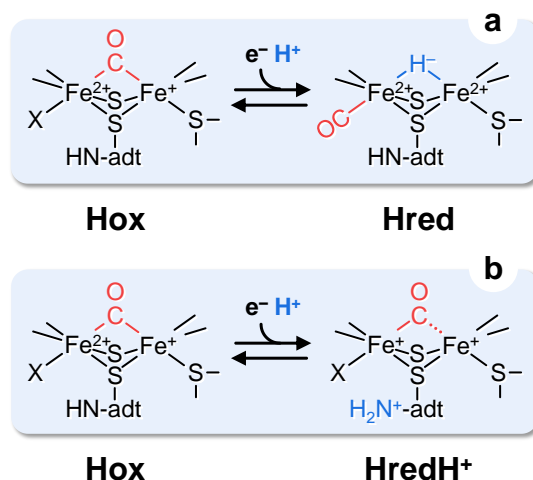
Figure 6 – Reduction and protonation of the Fe–Fe site. The two proposed models for the geometry of the reduced Fe−Fe site. In model a, PCET leads to formation of a Fe−Fe bridging hydride (μH⁻) and an apical CO at the distal iron ion instead of an open coordination site ('X'). In model b, PCET leads to protonation of the adt ligand (⁺NH₂) and a weakening of the μCO ligand (dashed line). This geometry, referred to as **HredH⁺**, may represent an intermediate in the **Hox →** **Hred** conversion. Note: as electrons enter the H-cluster *via* the [4Fe-4S] cluster, an Hred´-like intermediate might be involved in the conversion as well (not shown).

Illuminating H₂-reduced [FeFe]-hydrogenase with high intensity visible light under cryogenic conditions, a conversion of **Hred** and **Hsred** into H-cluster states with a terminal hydride similar to **Hhyd** has been noted.[48] The pH dependence or the carboxylic IR difference signature has not been evaluated, neither is the molecular mechanism of the conversion understood.[17] As the redox state of the [4Fe-4S] cluster differs in **Hred** and **Hsred** (**Figure 2C**), iron-sulfur photochemistry can be ruled out. Alternatively, it is tempting to explain the conversion to the presence of a photolabile Fe−Fe bridging hydride ligand (μH⁻) in **Hred** and **Hsred** (**Figure 6**, model a), reminiscent of the **Ni-C → Ni-L** transition discussed in Chapter 2.2. Under ambient conditions, the IR signature of **Hred** and **Hsred** is in good agreement with a μH⁻ geometry[3] and the formation

of a μH$^-$ ligand would explain the pH-dependent midpoint potentials for the **Hox → Hred** redox transition.[49,50] However, several authors demonstrated that **Hred** and **Hsred** maintain a 'semi-bridging' or fully-bridged CO ligand at cryogenic temperatures,[51,52] which would rule out the possibility of a μH$^-$ ligand (**Figure 6**, model b). To explain the pH dependence, a protonation of the aminodithiolate (adt) ligand has been proposed.[49] We assume that the so-called **HredH$^+$** state may represent an intermediate between **Hox** and **Hred**, kinetically trapped under cryogenic conditions not unlike **Ni-L** as an intermediate between **Ni-C** and **Ni-SI$_a$** (Chaper 2.2). The influence of temperature and whether **Hred** and **HredH$^+$** really originate from different H-cluster states is yet to decipher.[17]

3.2 Proton transfer during the catalytic cycle

In variance to **Hred´**, there is no way to trigger the accumulation of **Hred** over **Hox** 'naturally' by visible light; however, numerous applications of redox dyes have been reported.[53–55] Among these, 5'-carboxy eosin Y in combination with EDTA as a sacrificial electron donor[53] was found to facilitate an efficient photoreduction of the [FeFe]-hydrogenase from *Chlamydomonas reinhardtii* (*Cr*HydA1) when illuminated at 505 nm under ambient conditions.[8] Although **Hred** may represent an 'unready' H-cluster state (Chapter 3.3), its accumulation can be used to address changes in protonation and hydrogen-bonding in the catalytic PT pathway of [FeFe]-hydrogenase.

The FTIR difference spectrum in

Figure 7A depicts the conversion of **Hox** (negative bands) into **Hred** (positive bands). Less than 10% of other H-cluster states were detected. In comparison to the *Dv*MF [NiFe]-hydrogenase (**Figure 4**), no difference bands were observed in the frequency regime of 'dangling water' (3800 – 3600 cm^{-1}, not shown) or thioles (ν_{SH}, inset 1), which makes changes in protonation or hydrogen-

bonding involving individual water molecules or cysteine residues highly improbable.[8] In particular, the lack of SH difference signals is in conflict with a protonated adt ligand interacting with a cysteine *(i.e.*, C299 in *Cp*I), arguing in favor of **Hred** rather than **HredH$^+$** (**Figure 6**). This assignment is further supported by the lack of a μCO band, which is characteristic for **HredH$^+$**.[51,52] The frequency regime < 1750 cm^{-1} (inset 2) was found to be considerably more complex than in [NiFe]-hydrogenase.

Figure 7B depicts the **Hred – Hox** difference spectrum in hydrated and deuterated sample. Here, two negative and two positive bands suggest hydrogen-bonding changes involving carboxylic side chains (blue labels), which is supported by a shift to lower frequencies in the deuterated sample. The negative band at 1681 cm^{-1} was found to shift more drastically (magenta traces), reminiscent of the large H/D isotope effect observed with guanidium hydrochloride, which facilitates assignment to an arginine residue.
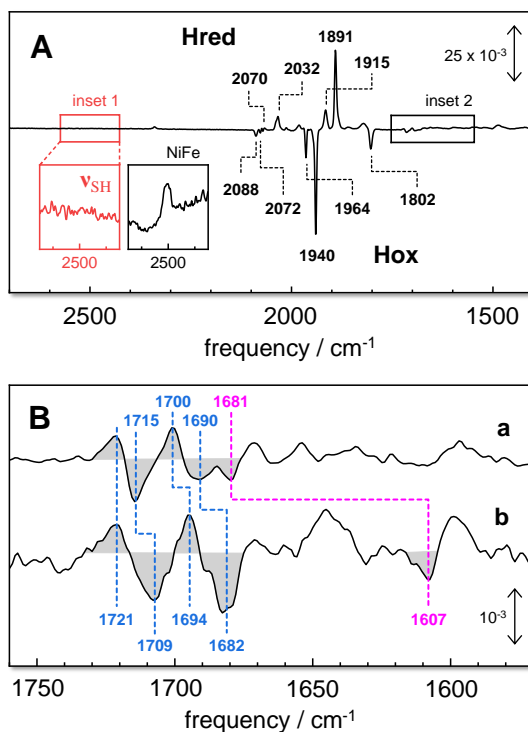
Figure 7 – FTIR difference spectra of the Hox to Hred transition. (A) FTIR difference spectrum for the accumulation of **Hred** over **Hox** as identified *via* the CO/CN⁻ bands of the H-cluster (black labels). No significant changes were observed in the OH regime (not shown) and SH regime (inset 1). For comparison, the SH difference signal from **Figure 4A** is depicted (NiFe, scaled by 1.5 to match the CO absorbance of cofactors). **(B)** Close-up of inset 2 in panel (A) for the same experiment on (a) hydrated and (b) deuterated [FeFe]-hydrogenase. Legend: $\nu_{CO/CN}$ (black), ν_{COOH} (blue), and arginine (magenta).

Several amino acid variants of *Cr*HydA1 were generated and crystallized to facilitate an experimental assignment of the FTIR difference spectra.[8,16] For example, the lack of the arginine side chain in *Cr*HydA1-R148A (eq. R286 in the [FeFe]-hydrogenase from *Clostridium*

*pasteurianum Cp*I) led to a disappearance of the band at 1681 cm^{-1} in **Hox**, which is in excellent agreement with the H/D effect (

Figure 7B) and suggests deprotonation of R148 in the formation of **Hred**. Analyzing the E144D variant (eq. R282 in *Cp*I), a pronounced up-shift of the band at 1721 cm^{-1} was observed in **Hred** that can be explained by the lack of a hydrogen-bonding contact with R148 as suggested by crystallographic analyses before.[16] Any variation of E141 (eq. R279 in *Cp*I) impeded accumulation of **Hred** over **Hox**. As none of the 'PT conservative' variants affected the 1715 cm^{-1}/ 1700 cm^{-1} difference signal, we assigned this feature to E141 and concluded an increase in hydrogen-bonding strength in **Hred** compared to **Hox**.

The spectroscopic analysis of the catalytic hydrogen-bonding network in [FeFe]-hydrogenase identified subtle differences between the oxidized and reduced enzyme.[8] **Figure 8** shows our model of the 'discontinued' PT that is characterized by the lack of hydrogen-bonding interactions between S319 and E279 in **Hox** (panel a, note the cleft). Upon one-electron reduction of the diiron site, a proton is subtracted from E279 and binds to the H-cluster, forming the transient **HredH$^+$** state (panel b). Then, re-protonation *via* R286$^+$ triggers the changes in the hydrogen-bonding network as shown in panel c. Instead of being involved in a hydrogen-bonding *trans* complex with a water molecule, E279 connects with S319 whereas E282 loses the hydrogen bond to the now deprotonated R286. We presume that re-protonation of R286 *via* the bulk solvent in **Hred** is precluded by the orientation of E279 and electrostatic repulsion.

Figure 8 – Proposed proton transfer mechanism of [FeFe]-hydrogenase. Infrared data suggest hydrogen-bonding contacts between $R286^+$, E282, and S319 in the **Hox** state (*Cp*I numbering, panel a). Crystallographic data allows concluding hydrogen-bonding between E279, W1, C299, and the adt ligand of the H-cluster. Panel b shows a potential intermediate, characterized by deprotonation of E141 and protonation of the reduced H-cluster (**HredH$^+$**). The later relaxes towards the **Hred** state (panel c). Moreover, the E279/W1 complex dissolves in favor of hydrogen bonding between E279, S319, and E282, which facilitates continuous PT.

In conclusion, the model of 'discontinued' PT as detailed in **Figure 8** provides a reasonable explanation how [FeFe]-hydrogenase distinguishes proton influx (H_2 release) from proton efflux (H_2 oxidation): in H_2 release direction, PT is driven by an increase of basicitiy of the H-cluster, *i.e.* upon reduction, and the transient subtraction of a proton from E141. In H_2 oxidation direction,

protons can leave the active site niche freely, *i.e.* triggered upon oxidation of the H-cluster, because the hydrogen-bonding environment allows for continuous PT.

3.3 Understanding [FeFe]-hydrogenase catalysis

Proton transfer determines the catalytic performance of [FeFe]-hydrogenase in multiple ways. Primarily, protons are educts in the H_2 release reaction and products of the H_2 oxidation reaction (**Eq. 1**) but the relation between [FeFe]-hydrogenase activity and proton concentration is arguably more complicated than this. For example, gas chromatographic analyses of solution assays show an increase of H_2 evolution activity going from alkaline to neutral pHs; however, the rate drops when the pH is lowered any further.[56] Such assays typically rely on dithionite as a sacrificial donor, which might explain the pH dependence. To this end, Ruth *et al.* reported a set-up that combines electrochemical reduction and chromatographic gas analysis and observed that the catalytic activity of [FeFe]-hydrogenase peaked at pH 6, independent of dithionite.[57]

In a recent study, we addressed the influence of pH on the accumulation of reduced H-cluster states under turnover conditions.[50] We noted a clear trend for **Hred** to dominate at pH < 7 and **Hred´** to dominate at pH > 7, confirming former observations.[47] This can explain the bell-shaped activity distribution as a function of pH: The preference for **Hred** under proton-rich conditions might indicate that the H-cluster forms an unready, H_2-inhibited geometry[58] upon PCET to the Fe−Fe active site, *e.g.* controlled by the low pK$_a$ of the glutamic acid residues in the PT pathway (**Figure 8**).[8] The water chain that connects the [4Fe-4S] cluster to the protein surface provides no such selectivity. Thus, **Hred´** is the main one-electron reduced H-cluster state under proton-poor conditions.[50] Following the model devised in ref. 3, site-selective protonation by PCET to the [4Fe-4S] cluster and Fe−Fe site allows [FeFe]-hydrogenase to switch between active-ready and unready H-cluster geometries, *e.g.* in the context of H_2 sensing.[59,60]

3.4 Alternative proton transfer pathways

Computational studies suggested three different PT pathways.[20,21] Pathway 1 resembles the trajectory discussed above (Chapter 3.2). Pathway 2 shares the cysteine residue with pathway 1 but branches at the water cluster. It includes several other water molecules, a serine, and a lysine residue near the protein surface. Pathway 3 is independent from pathway 1 and 2: originally, it was proposed by Juan Fontecilla-Camps *et al.* assuming a hydrogen bond between the distal CN^- ligand and a conserved lysine residue.[13] Pathway 3 includes two glutamic acid residues and several other water molecules.[21] A fourth pathway was considered first by John W. Peters and co-workers.[12] Here, a methionine residue near the adt ligand of the H-cluster may facilitate PT, as supported by site-direct mutagenesis and enzymology studies.[61]

While pathway 1 has been identified as the main catalytic PT trajectory,[16] alternative pathways may regulate PT in phylogenetically distinct [FeFe]-hydrogenases.[17] Such systems are largely unchartered, although first studies have emerged.[59,60] In the future, it will be exciting to investigate 'novel' [FeFe]-hydrogenases by FTIR difference spectroscopy to solve the puzzle that is catalytic PT.

4. Proton Transfer in Bimetallic Hydrogenase

[NiFe]-hydrogenase and [FeFe]-hydrogenase belong to the family of iron-sulfur enzymes but have evolved independently throughout evolution.[1] Nevertheless, the active site cofactors show a number of similarities, *e.g.* geometry and electronic structure, ligation motives, and metal hydride

chemistry. Bimetallic hydrogenases catalyze the same reaction (**Eq. 1**) and suffer from both CO and O_2 inhibition/deactivation, albeit to a different extent.[3,4] Moreover, convergent evolution shaped several conformities in the mechanism of PT. This includes a cysteine proximal to the active site cofactor, followed by a glutamic acid and a serine or threonine residue.[7,8] In [FeFe]-hydrogenase, the involvement of a small water cluster is undisputed (**Figure 8**) whereas respective water entities in [NiFe]-hydrogenase remain to be identified (**Figure 5**).

The independent FTIR analyses from our laboratories indicate hydrogen-bonding changes of the glutamic acid residue(s) in the PT pathway but no protonation differences, at least under steady-state conditions.[7,8] In [FeFe]-hydrogenase, hydrogen-bonding changes influence the directionality of PT whereas no spectral differences were observed with the proximal cysteine residue. This is in marked contrast to [NiFe]-hydrogenase. Here, the protonation differences of the proximal cysteine may be the reason why [NiFe]-hydrogenase show a clear bias towards H_2 oxidation.[1] We propose that the proximal cysteine at the Ni−Fe cofactor serves as *proton loading site* while the proximal cysteine close to the Fe−Fe site functions as flexible *proton relay*. In conclusion, FTIR difference spectroscopy has been demonstrated to serve as a powerful tool detecting subtle structural changes in the PT pathway of [NiFe]- and [FeFe]-hydrogenases, despite the lack of a dedicated chromophore. Combined with high-resolution crystal structures, a conclusive and molecular-detailed description of PT in bimetallic hydrogenases is achieved.

5. Acknowledgements

6. References

(1)   Lubitz, W.; Ogata, H.; Rüdiger, O.; Reijerse, E. Hydrogenases. *Chem. Rev.* **2014**, *114* (8), 4081–4148. https://doi.org/10.1021/cr4005814.

(2)   Tai, H.; Higuchi, Y.; Hirota, S. Comprehensive Reaction Mechanisms at and near the Ni-Fe Active Sites of [NiFe] Hydrogenases. *Dalt. Trans.* **2018**, *47* (13), 4408–4423. https://doi.org/10.1039/c7dt04910b.

(3)   Haumann, M.; Stripp, S. T. The Molecular Proceedings of Biological Hydrogen Turnover. *Acc. Chem. Res.* **2018**, *51* (8), 1755–1763. https://doi.org/10.1021/acs.accounts.8b00109.

(4)   Tai, H.; Hirota, S. Mechanism and Application of the Catalytic Reaction of [NiFe] Hydrogenase: Recent Developments. *ChemBioChem* **2020**, *21* (11), 1573–1581. https://doi.org/10.1002/cbic.202000058.

(5)   Wittkamp, F.; Senger, M.; Stripp, S. T.; Apfel, U.-P. [FeFe]-Hydrogenases: Recent Developments and Future Perspectives. *Chem. Commun.* **2018**, *54* (47), 5934–5942. https://doi.org/10.1039/C8CC01275J.

(6)   Schilter, D.; Camara, J. M.; Huynh, M. T.; Hammes-Schiffer, S.; Rauchfuss, T. B. Hydrogenase Enzymes and Their Synthetic Models: The Role of Metal Hydrides. *Chem. Rev.* **2016**, *116* (15), 8693–8749. https://doi.org/10.1021/acs.chemrev.6b00180.

(7)   Tai, H.; Nishikawa, K.; Higuchi, Y.; Mao, Z.-W.; Hirota, S. Cysteine SH and Glutamate COOH Contributions to [NiFe] Hydrogenase Proton Transfer Revealed by Highly Sensitive FT-IR Spectroscopy. *Angew. Chemie Int. Ed.* **2019**, *58* (38), 13285–13290.

https://doi.org/10.1002/anie.201904472.

(8)   Senger, M.; Eichmann, V.; Laun, K.; Duan, J.; Wittkamp, F.; Knör, G.; Apfel, U.-P.; Happe, T.; Winkler, M.; Heberle, J.; Stripp, S. T.; Timo, S. How [FeFe]-Hydrogenase Facilitates Bidirectional Proton Transfer. *J. Am. Chem. Soc.* **2019**, *141* (43), 17394–17403. https://doi.org/10.1021/jacs.9b09225.

(9)   Ogata, H.; Nishikawa, K.; Lubitz, W. Hydrogens Detected by Subatomic Resolution Protein Crystallography in a [NiFe] Hydrogenase. *Nature* **2015**, *520* (7548), 571–574. https://doi.org/10.1038/nature14110.

(10)   Volbeda, A.; Charon, M. H.; Piras, C.; Hatchikian, E. C.; Frey, M.; Fontecilla-Camps, J. C. Crystal Structure of the Nickel–Iron Hydrogenase from Desulfovibrio Gigas. *Nature* **1995**, *373* (6515), 580–587. https://doi.org/10.1038/373580a0.

(11)   Ash, P. A.; Hidalgo, R.; Vincent, K. A. Proton Transfer in the Catalytic Cycle of [NiFe] Hydrogenases: Insight from Vibrational Spectroscopy. *ACS Catal.* **2017**, *7* (4), 2471–2485. https://doi.org/10.1021/acscatal.6b03182.

(12)   Peters, J. W.; Lanzilotta, W. N.; Lemon, B. J.; Seefeldt, L. C. X-Ray Crystal Structure of the Fe-Only Hydrogenase (CpI) from Clostridium Pasteurianum to 1.8 Angstrom Resolution. *Science* **1998**, *282* (5395), 1853–1858. https://doi.org/10.1126/science.282.5395.1853.

(13)   Nicolet, Y.; Piras, C.; Legrand, P.; Hatchikian, C. E.; Fontecilla-Camps, J. C. Desulfovibrio Desulfuricans Iron Hydrogenase: The Structure Shows Unusual Coordination to an Active Site Fe Binuclear Center. *Structure* **1999**, *7* (1), 13–23. https://doi.org/10.1016/S0969-2126(99)80005-7.

(14)   Silakov, A.; Wenk, B.; Reijerse, E.; Lubitz, W. 14N HYSCORE Investigation of the H-

Cluster of [FeFe] Hydrogenase: Evidence for a Nitrogen in the Dithiol Bridge. *Phys. Chem. Chem. Phys.* **2009**, *11* (31), 6553–6554. https://doi.org/10.1039/b913085n.

(15)   Winkler, M.; Esselborn, J.; Happe, T. Molecular Basis of [FeFe]-Hydrogenase Function: An Insight into the Complex Interplay between Protein and Catalytic Cofactor. *Biochim. Biophys. Acta* **2013**, *1827* (8–9), 974–985. https://doi.org/10.1016/j.bbabio.2013.03.004.

(16)   Duan, J.; Senger, M.; Esselborn, J.; Engelbrecht, V.; Wittkamp, F.; Apfel, U.-P.; Hofmann, E.; Stripp, S. T.; Happe, T.; Winkler, M. Crystallographic and Spectroscopic Assignment of the Proton Transfer Pathway in [FeFe]-Hydrogenases. *Nat. Commun.* **2018**, *9*, 4726. https://doi.org/10.1038/s41467-018-07140-x.

(17)   Land, H.; Senger, M.; Berggren, G.; Stripp, S. T. Current State of [FeFe]-Hydrogenase Research - Biodiversity and Spectroscopic Investigations. *ACS Catal.* **2020**, *10*, 7069–7086. https://doi.org/10.1021/acscatal.0c01614.

(18)   Teixeira, V. H.; Soares, C. M.; Baptista, A. M. Proton Pathways in a [NiFe]-Hydrogenase: A Theoretical Study. *Proteins Struct. Funct. Genet.* **2007**, *70* (3), 1010–1022. https://doi.org/10.1002/prot.21588.

(19)   Galván, I. F.; Volbeda, A.; Fontecilla-Camps, J. C.; Field, M. J. A QM/MM Study of Proton Transport Pathways in a [NiFe] Hydrogenase. *Proteins Struct. Funct. Genet.* **2008**, *73* (1), 195–203. https://doi.org/10.1002/prot.22045.

(20)   Long, H.; King, P. W.; Chang, C. H. Proton Transport in Clostridium Pasteurianum [FeFe] Hydrogenase I: A Computational Study. *J. Phys. Chem. B* **2014**, *118* (4), 890–900. https://doi.org/10.1021/jp408621r.

(21)   Ginovska-Pangovska, B.; Ho, M.-H.; Linehan, J. C.; Cheng, Y.; Dupuis, M.; Raugei, S.; Shaw, W. J. Molecular Dynamics Study of the Proposed Proton Transport Pathways in

[FeFe]-Hydrogenase. *Biochim. Biophys. Acta* **2014**, *1837* (1), 131–138. https://doi.org/10.1016/j.bbabio.2013.08.004.

(22)   Lorenz-Fonfria, V. A. Infrared Difference Spectroscopy of Proteins: From Bands to Bonds. *Chem. Rev.* **2020**, *120* (7), 3466–3576. https://doi.org/10.1021/acs.chemrev.9b00449.

(23)   Tai, H.; Xu, L.; Inoue, S.; Nishikawa, K.; Higuchi, Y.; Hirota, S. Photoactivation of the Ni-SIr State to the Ni-SIa State in [NiFe] Hydrogenase: FT-IR Study on the Light Reactivity of the Ready Ni-SIr State and as-Isolated Enzyme Revisited. *Phys. Chem. Chem. Phys.* **2016**, *18* (32), 22025–22030. https://doi.org/10.1039/c6cp04628b.

(24)   Tai, H.; Nishikawa, K.; Suzuki, M.; Higuchi, Y.; Hirota, S. Control of the Transition between Ni-C and Ni-SIastates by the Redox State of the Proximal Fe-S Cluster in the Catalytic Cycle of [NiFe] Hydrogenase. *Angew. Chemie - Int. Ed.* **2014**, *53* (50), 13817–13820. https://doi.org/10.1002/anie.201408552.

(25)   Tai, H.; Xu, L.; Nishikawa, K.; Higuchi, Y.; Hirota, S. Equilibrium between Inactive Ready Ni-SIr and Active Ni-SIa States of [NiFe] Hydrogenase Studied by Utilizing Ni-SIr-to-Ni-SIa Photoactivation. *Chem. Commun.* **2017**, *53* (75), 10444–10447. https://doi.org/10.1039/c7cc06061k.

(26)   Bell, R. P. Recent Advances in the Study of Kinetic Hydrogen Isotope Effects. *Chem. Soc. Rev.* **1974**, *3* (4), 513–544. https://doi.org/10.1039/CS9740300513.

(27)   Dong, G.; Ryde, U. Protonation States of Intermediates in the Reaction Mechanism of [NiFe] Hydrogenase Studied by Computational Methods. *J. Biol. Inorg. Chem.* **2016**, *21* (3), 383–394. https://doi.org/10.1007/s00775-016-1348-9.

(28)   Dementin, S.; Burlat, B.; De Lacey, A. L.; Pardo, A.; Adryanczyk-Perrier, G.; Guigliarelli, B.; Fernandez, V. M.; Rousset, M. A Glutamate Is the Essential Proton Transfer Gate during

the Catalytic Cycle of the [NiFe] Hydrogenase. *J. Biol. Chem.* **2004**, *279* (11), 10508–10513. https://doi.org/10.1074/jbc.M312716200.

(29)   Greene, B. L.; Vansuch, G. E.; Wu, C. H.; Adams, M. W. W.; Dyer, R. B. Glutamate Gated Proton-Coupled Electron Transfer Activity of a [NiFe]-Hydrogenase. *J. Am. Chem. Soc.* **2016**, *138* (39), 13013–13021. https://doi.org/10.1021/jacs.6b07789.

(30)   Evans, R. M.; Ash, P. A.; Beaton, S. E.; Brooke, E. J.; Vincent, K. A.; Carr, S. B.; Armstrong, F. A. Mechanistic Exploitation of a Self-Repairing, Blocked Proton Transfer Pathway in an O2-Tolerant [NiFe]-Hydrogenase. *J. Am. Chem. Soc.* **2018**, *140* (32), 10208–10220. https://doi.org/10.1021/jacs.8b04798.

(31)   Gebler, A.; Burgdorf, T.; De Lacey, A. L.; Rüdiger, O.; Martinez-Arias, A.; Lenz, O.; Friedrich, B. Impact of Alterations near the [NiFe] Active Site on the Function of the H2 Sensor from Ralstonia Eutropha. *FEBS J.* **2007**, *274* (1), 74–85. https://doi.org/10.1111/j.1742-4658.2006.05565.x.

(32)   Weber, K.; Krämer, T.; Shafaat, H. S.; Weyhermüller, T.; Bill, E.; Van Gastel, M.; Neese, F.; Lubitz, W. A Functional [NiFe]-Hydrogenase Model Compound That Undergoes Biologically Relevant Reversible Thiolate Protonation. *J. Am. Chem. Soc.* **2012**, *134* (51), 20745–20755. https://doi.org/10.1021/ja309563p.

(33)   Yu, X.; Pang, M.; Zhang, S.; Hu, X.; Tung, C. H.; Wang, W. Terminal Thiolate-Dominated H/D Exchanges and H2 Release: Diiron Thiol-Hydride. *J. Am. Chem. Soc.* **2018**, *140* (36), 11454–11463. https://doi.org/10.1021/jacs.8b06996.

(34)   Tai, H.; Nishikawa, K.; Inoue, S.; Higuchi, Y.; Hirota, S. FT-IR Characterization of the Light-Induced Ni-L2 and Ni-L3 States of [NiFe] Hydrogenase from Desulfovibrio Vulgaris Miyazaki F. *J. Phys. Chem. B* **2015**, *119* (43), 13688–13674.

https://doi.org/10.1021/acs.jpcb.5b03075.

(35) Brecht, M.; Van Gastel, M.; Buhrke, T.; Friedrich, B.; Lubitz, W. Direct Detection of a Hydrogen Ligand in the [NiFe] Center of the Regulatory H2-Sensing Hydrogenase from Ralstonia Eutropha in Its Reduced State by HYSCORE and ENDOR Spectroscopy. *J. Am. Chem. Soc.* **2003**, *125* (43), 13075–13083. https://doi.org/10.1021/ja036624x.

(36) Evans, R. M.; Brooke, E. J.; Wehlin, S. A. M.; Nomerotskaia, E.; Sargent, F.; Carr, S. B.; Phillips, S. E. V.; Armstrong, F. A. Mechanism of Hydrogen Activation by [NiFe] Hydrogenases. *Nat. Chem. Biol.* **2016**, *12* (1), 46–50. https://doi.org/10.1038/nchembio.1976.

(37) Tombolelli, D.; Mroginski, M. A. Proton Transfer Pathways between Active Sites and Proximal Clusters in the Membrane-Bound [NiFe] Hydrogenase. *J. Phys. Chem. B* **2019**, *123* (16), 3409–3420. https://doi.org/10.1021/acs.jpcb.9b00617.

(38) Frielingsdorf, S.; Fritsch, J.; Schmidt, A.; Hammer, M.; Löwenstein, J.; Siebert, E.; Pelmenschikov, V.; Jaenicke, T.; Kalms, J.; Rippers, Y.; Lendzian, F.; Zebger, I.; Teutloff, C.; Kaupp, M.; Bittl, R.; Hildebrandt, P.; Friedrich, B.; Lenz, O.; Scheerer, P. Reversible [4Fe-3S] Cluster Morphing in an O 2 -Tolerant [NiFe] Hydrogenase. *Nat. Chem. Biol.* **2014**, *10* (5), 378–385. https://doi.org/10.1038/nchembio.1500.

(39) Lemon, B. J.; Peters, J. W. Photochemistry at the Active Site of the Carbon Monoxide Inhibited Form of the Iron-Only Hydrogenase (CpI). *J. Am. Chem. Soc.* **2000**, *122* (15), 3793–3794. https://doi.org/10.1021/ja9943703.

(40) Bennett, B.; Lemon, B. J.; Peters, J. W. Reversible Carbon Monoxide Binding and Inhibition at the Active Site of the Fe-Only Hydrogenase. *Biochemistry* **2000**, *39* (25), 7455–7460.

(41)   Chen, Z.; Lemon, B. J.; Huang, S.; Swartz, D. J.; Peters, J. W.; Bagley, K. A. Infrared Studies of the CO-Inhibited Form of the Fe-Only Hydrogenase from Clostridium Pasteurianum I: Examination of Its Light Sensitivity at Cryogenic Temperatures. *Biochemistry* **2002**, *41* (6), 2036–2043. https://doi.org/10.1021/bi011510o.

(42)   Albracht, S. P. J.; Roseboom, W.; Hatchikian, E. C. The Active Site of the [FeFe]-Hydrogenase from Desulfovibrio Desulfuricans. I. Light Sensitivity and Magnetic Hyperfine Interactions as Observed by Electron Paramagnetic Resonance. *J. Biol. Inorg. Chem.* **2006**, *11* (1), 88–101. https://doi.org/10.1007/s00775-005-0039-8.

(43)   Roseboom, W.; De Lacey, A. L.; Fernandez, V. M.; Hatchikian, E. C.; Albracht, S. P. J. The Active Site of the [FeFe]-Hydrogenase from Desulfovibrio Desulfuricans. II. Redox Properties, Light Sensitivity and CO-Ligand Exchange as Observed by Infrared Spectroscopy. *J. Biol. Inorg. Chem.* **2006**, *11* (1), 102–118. https://doi.org/10.1007/s00775-005-0040-2.

(44)   Sensi, M.; Baffert, C.; Fradale, L.; Gauquelin, C.; Soucaille, P.; Meynial-Salles, I.; Bottin, H.; De Gioia, L.; Bruschi, M.; Fourmond, V.; Léger, C.; Bertini, L. Photoinhibition of FeFe Hydrogenase. *ACS Catal.* **2017**, *7* (10), 7378–7387. https://doi.org/10.1021/acscatal.7b02252.

(45)   Katz, S.; Noth, J.; Horch, M.; Shafaat, H. S.; Happe, T.; Hildebrandt, P.; Zebger, I. Vibrational Spectroscopy Reveals the Initial Steps of Biological Hydrogen Evolution. *Chem. Sci.* **2016**, *7*, 6746–6752. https://doi.org/10.1039/C6SC01098A.

(46)   Senger, M.; Laun, K.; Wittkamp, F.; Duan, J.; Haumann, M.; Happe, T.; Winkler, M.; Apfel, U.-P.; Stripp, S. T. Proton-Coupled Reduction of the Catalytic [4Fe-4S] Cluster in [FeFe]-Hydrogenases. *Angew. Chemie Int. Ed.* **2017**, *56* (52), 16503–16506.

https://doi.org/10.1002/anie.201709910.

(47)   Senger, M.; Mebs, S.; Duan, J.; Shulenina, O.; Laun, K.; Kertess, L.; Wittkamp, F.; Apfel,
U.-P.; Happe, T.; Winkler, M.; Haumann, M.; Stripp, S. T. Protonation/Reduction
Dynamics at the [4Fe–4S] Cluster of the Hydrogen-Forming Cofactor in [FeFe]-
Hydrogenases. *Phys. Chem. Chem. Phys.* **2018**, *20* (5), 3128–3140.
https://doi.org/10.1039/C7CP04757F.

(48)   Lorent, C.; Katz, S.; Duan, J.; Julia Kulka, C.; Caserta, G.; Teutloff, C.; Yadav, S.; Apfel,
U.-P.; Winkler, M.; Happe, T.; Horch, M.; Zebger, I. Shedding Light on Proton and Electron
Dynamics in [FeFe] Hydrogenases. *J. Am. Chem. Soc.* **2020**, *142* (12), 5493–5497.
https://doi.org/10.1021/jacs.9b13075.

(49)   Sommer, C.; Adamska-Venkatesh, A.; Pawlak, K.; Birrell, J. A.; Rüdiger, O.; Reijerse, E.
J.; Lubitz, W. Proton Coupled Electronic Rearrangement within the H-Cluster as an
Essential Step in the Catalytic Cycle of [FeFe] Hydrogenases. *J. Am. Chem. Soc.* **2017**, *139*
(4), 1440−1443. https://doi.org/10.1021/jacs.6b12636.

(50)   Laun, K.; Baranova, I.; Duan, J.; Wittkamp, F.; Apfel, U.-P.; Happe, T.; Senger, M.; Stripp,
S. T. Site-Selective Protonation of the Catalytic Cofactor in [FeFe]-Hydrogenase.
ChemRxiv **2019**. https://doi.org/https://doi.org/10.26434/chemrxiv.9970571.v2.

(51)   Ratzloff, M. W.; Artz, J. H.; Mulder, D. W.; Collins, R. T.; Furtak, T. E.; King, P. W. CO-
Bridged H-Cluster Intermediates in the Catalytic Mechanism of [FeFe]-Hydrogenase CaI.
J. Am. Chem. Soc. **2018**, *140* (24), 7623–7628. https://doi.org/10.1021/jacs.8b03072.

(52)   Birrell, J. A.; Pelmenschikov, V.; Mishra, N.; Wang, H.; Yoda, Y.; Rauchfuss, T. B.;
Cramer, S. P.; Lubitz, W.; Debeer, S. Spectroscopic and Computational Evidence That
[FeFe] Hydrogenases Operate Exclusively with CO-Bridged Intermediates Spectroscopic

and Computational Evidence That [FeFe] Hydrogenases Operate Exclusively with CO-Bridged. *J. Am. Chem. Soc.* **2020**, *142* (1), 222–232. https://doi.org/10.1021/jacs.9b09745.

(53)   Adam, D.; Bösche, L.; Castaneda-Losada, L.; Winkler, M.; Apfel, U.-P.; Happe, T. Sunlight-Dependent Hydrogen Production by Photosensitizer / Hydrogenase Systems. *ChemSusChem* **2017**, *10* (5), 894–902. https://doi.org/10.1002/cssc.201601523.

(54)   Greene, B. L.; Schut, G. J.; Adams, M. W. W.; Dyer, R. B. Pre-Steady-State Kinetics of Catalytic Intermediates of an [FeFe]-Hydrogenase. *ACS Catal.* **2017**, *7*, 2145–2150. https://doi.org/10.1021/acscatal.6b03276.

(55)   Sanchez, M. L. K.; Sommer, C.; Reijerse, E.; Birrell, J. A.; Lubitz, W.; Dyer, R. B. Investigating the Kinetic Competency of CrHydA1 [FeFe] Hydrogenase Intermediate States via Time-Resolved Infrared Spectroscopy. *J. Am. Chem. Soc.* **2019**, *141* (40), 16064–16070. https://doi.org/10.1021/jacs.9b08348.

(56)   Happe, T.; Naber, J. D. Isolation, Characterization and N-terminal Amino Acid Sequence of Hydrogenase from the Green Alga Chlamydomonas Reinhardtii. *Eur. J. Biochem.* **1993**, *214* (2), 475–481. https://doi.org/10.1111/j.1432-1033.1993.tb17944.x.

(57)   Ruth, J. C.; Milton, R. D.; Gu, W.; Spormann, A. M. Enhanced Electrosynthetic Hydrogen Evolution by Hydrogenases Embedded in a Redox-Active Hydrogel. *Chem. – A Eur. J.* **2020**, in press. https://doi.org/10.1002/chem.202000750.

(58)   Duan, J.; Mebs, S.; Laun, K.; Wittkamp, F.; Heberle, J.; Hofmann, E.; Apfel, U.-P.; Winkler, M.; Senger, M.; Haumann, M.; Stripp, S. T. Geometry of the Catalytic Active Site in [FeFe]-Hydrogenase Is Determined by Hydrogen Bonding and Proton Transfer. *ACS Catal.* **2019**, *9* (10), 9140–9149. https://doi.org/10.1021/acscatal.9b02203.

(59)   Chongdar, N.; Birrell, J. A.; Pawlak, K.; Sommer, C.; Reijerse, E. J.; Rüdiger, O.; Lubitz,

W.; Ogata, H. Unique Spectroscopic Properties of the H-Cluster in a Putative Sensory [FeFe] Hydrogenase. *J. Am. Chem. Soc.* **2018**, *140* (3), 1057−1068. https://doi.org/10.1021/jacs.7b11287.

(60)   Land, H.; Ceccaldi, P.; Mészáros, L. S.; Lorenzi, M.; Redman, H. J.; Senger, M.; Stripp, S. T.; Berggren, G. Discovery of Novel [FeFe]-Hydrogenases for Biocatalytic H2-Production. *Chem. Sci.* **2019**, *10* (43), 9941–9948. https://doi.org/10.1039/c9sc03717a.

(61)   Knörzer, P.; Silakov, A.; Foster, C. E.; Armstrong, F. A.; Lubitz, W.; Happe, T. Importance of the Protein Framework for Catalytic Activity of [FeFe]-Hydrogenases. *J. Biol. Chem.* **2012**, *287* (2), 1489–1499. https://doi.org/10.1074/jbc.M111.305797.